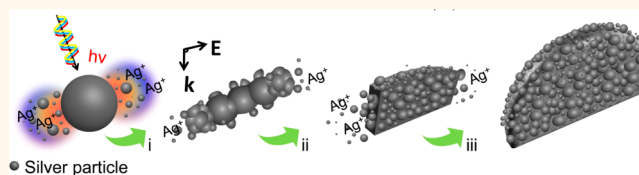


Surface-Plasmon-Mediated Programmable Optical Nanofabrication of an Oriented Silver Nanoplate

Bin-Bin Xu,[†] Lei Wang,[†] Zhuo-Chen Ma,[†] Ran Zhang,[†] Qi-Dai Chen,^{†,*} Chao Lv,[†] Bing Han,[†] Xin-Ze Xiao,[†] Xu-Lin Zhang,[†] Yong-Lai Zhang,[†] Kosei Ueno,[§] Hiroaki Misawa,^{§,*} and Hong-Bo Sun^{†,*,*}

[†]State Key Laboratory on Integrated Optoelectronics, College of Electronic Science and Engineering, Jilin University, Changchun 130012, China, [‡]College of Physics, Jilin University, Changchun 130023, China, and [§]Research Institute for Electronic Science, Hokkaido University, Kita-Ku, Sapporo, Hokkaido 001-0021, Japan

ABSTRACT We report polarized femtosecond laser-light-mediated growth and programmable assembly of photoreduced silver nanoparticles into triply hierarchical micropatterns. Formation of erected arrays of nanoplates with a thickness as small as $\lambda/27$ (λ , the writing laser wavelength) level is demonstrated. The growth mechanism of nanoplates has been clarified: (i) the excited surface



plasmons enhance the local electric field and lead to spatially selective growth of silver atoms at the opposite ends of dipoles induced on early created silver seeds; (ii) the optical attractive force overcomes electrostatic repulsion in the enhanced local electric field to assemble the silver nanoparticles directly. The triply hierarchical micropattern shape and location, the nanoplate orientation, and thickness are all attained in controlled fashion.

KEYWORDS: surface plasmons · silver · nanoplate · laser nanofabrication · SERS

Silver is considered particularly important due to its surface plasmon (SP) resonance wavelength at the visible spectral range and therefore is suitable for surface-enhanced Raman scattering (SERS)^{1–5} and tip-enhanced Raman scattering (TERS),^{6,7} photocatalysis,⁸ and plasmonics.⁹ Various nanofabrication technologies were adopted to produce silver nanostructures. Chemical approaches featuring bottom-up production of nanostructures,¹⁰ including controlled reduction, seed-mediated growth, and template-directed growth, are advantageous in individual particle shape control and rapid production of a large amount of samples, but the capability of spatially arranging nanostructures according to the requirements of device functions is apparently insufficient. In contrast, the nanofeatures in top-down structures produced by, for example, electron beam lithography, focused ion beam lithography, and nanosphere lithography are generally precisely designed,^{11–13} but the processing is restrained by usage of photomasks, application solely to limited material species, and restrained geometries. Optical nanofabrication has been demonstrated as an efficient

technology in designing and achieving complex metal structures with nanometer accuracy either by pursuit of short-wavelength lasers down to extra ultraviolet to X-ray wavebands,¹⁴ nonlinear light–matter interactions including photon tunneling in near-field optics,^{7,15,16} or multiphoton absorption in femtosecond laser direct writing.^{17–21} Especially in view of the fabrication precision, the designability of target structures, and the universality of useful materials, femtosecond laser direct writing is a relatively better choice, as proved by the enabled devices of microelectrical,²² micro-optical,^{23,24} micromechanical,²⁵ and microfluidic functions.^{26,27}

Femtosecond laser-induced photoreduction of metal ions is an important optical method for fabricating nanostructures, by which three-dimensional (3D) nanowiring and 3D metal structures are realized. The laser-induced photochemical deposition of silver patterns is generally a nonlinear absorption process; typically, when a single photon does not have enough energy to excite an electron from the valence to the conduction band, absorption of laser energy can occur through a nonlinear process,

* Address correspondence to chenqd@jlu.edu.cn, misawa@es.hokudai.ac.jp, hbsun@jlu.edu.cn.

Received for review December 26, 2013 and accepted June 4, 2014.

Published online June 04, 2014
10.1021/nn5029345

© 2014 American Chemical Society

which is known as multiphoton absorption.²⁸ One of the most important issues for femtosecond laser-induced fabrication of metal structures is the realization of 3D structure and high resolution. For example, Kawata *et al.* reported fabrication of electrically conductive silver wires with a minimum width of 400 nm and 3D silver microstructures by using silver nitrate aqueous solution with coumarin 440 as a two-photon sensitive dye.²⁹ Three-dimensional continuous metallic structures were fabricated by direct laser writing in polymer composites containing metal nanoparticles or metal salts.^{26,27} A technology of flexible nanowiring of metal on nonplanar substrates by femtosecond laser-induced electroless plating from metal ion precursors was also demonstrated, by which a microheater was integrated at the bed of the microfluidic chip channel.²² These methods mainly depend on absorbing photons to provide energies to induce photoreduction and accelerate the reaction process occurring at limited microvolume of the laser focal spot. By now, through controlling the laser power according to the reaction threshold or inducing inhibitor molecules, the resolution could be increased beyond the optical diffraction limit. Although a resolution of 20 nm in photopolymerization course through self-smoothing effect was reported, the highest resolution obtained by TPA-induced fabrication of metal structures from an ion precursor solution is about 100 nm.³⁰

Conversion of light into surface plasmon waves (SPs) leads to a significant wavelength reduction,³¹ considered to be a promising avenue toward super-resolution imaging,³² high-accuracy sensing,^{33,34} and on-chip optical interconnection.^{35,36} The SPs based on noble metals also play a crucial role in modification of molecular wave functions,³⁷ photosensitization in cancer therapy,³⁸ and enhancement of solar cell power conversion.^{39,40} Motion control of electrons by local field-enhanced SPs fields built in semiconducting or metallic nanostructures in terms of their shape, size, and periodicity of arrangement has been fully demonstrated.^{41–43} This scheme, however, has not been utilized for optical nanofabrication but limited examples of efforts in photochemical research; for example, Mirkin *et al.* introduced the concept of plasmonic seed-mediated triangular nanoprism shaping,^{44,45} and depending on the illumination wavelengths chosen, the plasmon excitations led either to fusion of nanoprisms in an edge-selective manner or to the growth of the nanoprisms until they reached a light-controlled final size. This method has been widely used to synthesize silver nanoprisms and other related structures (*e.g.*, nanodisks or truncated prisms).^{46,47} Tatsuma *et al.* reported the distribution of plasmon-induced charge separation sites at the Ag nanorod–TiO₂ interface.^{48,49} The charge separation sites are localized in almost the same way as electric fields around the nanorods, indicating that the charge separation is induced or

promoted by the localized electric fields which facilitate application of the charge separation to nanofabrication and other nanolocalized photoelectrochemical reactions.⁴⁸ Misawa *et al.* demonstrated for the first time that nanoparticle plasmons can induce a detectable nanowire polymerization under irradiation by incoherent continuous-wave (CW) sources. Two-photon polymerization (TPP) of the photoresist surrounding the nanoparticles was found in the high plasmonic field regions after irradiation by an incoherent light source, demonstrating that two-photon absorption (TPA) triggered a photochemical reaction without a laser source.^{50,51}

Despite the broad studies on surface plasmonics and the versatility of laser nanofabrication technologies, SPs-induced local field enhancement has not yet been thought of as an effective means for assisting optical fabrication of metal nanostructures. Herein, we report polarized femtosecond laser-light-mediated growth and programmable assembly of photo-reduced silver nanoparticles into nanoplates and micropatterns, during which the laser provides energy, optical force, and spatial resolution, which we call an optical dynamic assembly process. The fabricating system functions as an Otto configuration prism coupling system and was sufficient to excite SPs at the interface between the metal and the lower-index precursory solution.⁵² As far as we know, it is the first report of the formation of an erected array of nanoplates with a thickness of tens of nanometers as small as $\lambda/27$ (λ , the writing laser wavelength) level, and it is attributed to spatially selective growth of silver atoms at the opposite ends of dipoles induced by highly localized and greatly enhanced electric fields on early created silver seeds. The orientation of the nanoplates has a strict dependence with the laser polarization direction.

RESULTS AND DISCUSSION

Figure 1a shows the scheme we proposed for surface-plasmon-mediated optical nanofabrication of silver, where the 800 nm femtosecond laser pulses, with a width of 120 fs, were tightly focused on the interface between substrate and silver precursor solution prepared from silver nitrate, ammonia, and trisodium citrate which acts as both capping agent and reducing agent.²² The absence of absorption at 800 nm, the wavelength of applied laser (Supporting Information Figure S1), indicates that the photoreduction of silver ions is a multiphoton absorption (MPA) process, which benefits both (i) the deep transmission of the laser beam into the solution to reach the substrate surface with negligible power loss, and (ii) the high localization of the light–matter interaction volume, implying a high fabrication spatial resolution. As a representative illustration, a silver micropattern (Figure 1c, mascot of World Expo Shanghai 2010) was processed by three-layer scanning of the laser focal spot according to the

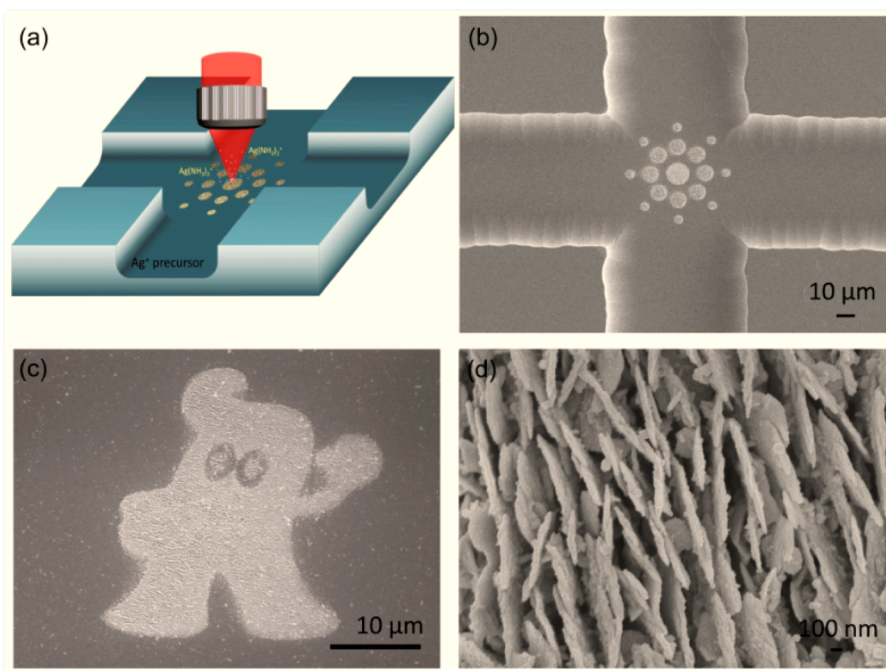


Figure 1. Surface-plasmon-mediated programmable optical nanofabrication of silver. (a) Scheme of femtosecond laser direct writing of silver triply hierarchical structures on a substrate. (b) SEM image of a Ag micropattern (the mascot of World Expo Shanghai 2010). (c) Locally magnified SEM image of the mascot. (d) SEM image of a silver circle array patterned on the bed at the intersection of two microchannels.

designed program. In each layer of the writing, the planar pattern program itself was kept identical but the laser focal spot was vertically lifted for a distance, typically 50 nm. As a result of the unique 3D laser processing capability, the fabrication was not limited to flat surfaces but possibly conducted in deep channels (Figure 1a). For example, the silver sphere array with different diameters of 4.5, 8.5, and 12 μm were arranged at the intersections of two 30 μm deep microchannels (Figure 1b), which may serve as an integrated SERS monitor in a microfluidic system to be shown later. The capability of programmable assembly of the photoreduced nanoparticles is ensured by the high-precision pinpoint laser writing scheme, which is not possibly fulfilled in various chemical self-organization processes. The patterns (Figure 1b,c) are considered as the first level of a triply hierarchical structure. As second level features, it is interesting to recognize from the magnified scanning electron microscopic (SEM) image (Figure 1d) that the micropatterns are actually composed of subwavelength nanoplates. They are perpendicular to the substrate and possess a thickness on the order of several tens of nanometers, which is one-tenth of the applied laser wavelength, and such small feature sizes have not been reported in laser-fabricated metal structures.

The array of the erected nanoplates is apparently different from the periodic structures created by interference, either between the incident laser beams or between the incident beam and its excited waves, where patterns are replicas of light intensity

redistributions, and the structure periods depend in principle on the laser wavelength and the beam incident angles. Here, we attribute the nanoplate array production to local field enhancement induced by SP mode on silver particles. The initial silver nanoparticles serving as seeds were produced in the first-layer laser scanning from the precursory solution through the MPA process, which is similar to the silver/gold microstructures through a path of dot-by-dot and line-by-line reported before;¹⁸ in the course of second-layer laser scanning, SP fields were significantly excited and established on the seeds, launching directional growth along the dipole ends by attracting atoms that were photoreduced in solution and the ripples and nanoplates were formed progressively (Figure 2c). Nanoparticles are able to act as an electron storage and transfer medium when the SPs are generated and there is an increase of the chemical reactivity on its surface.^{53,54} Hence, silver ions might more easily be reduced on the nanoparticle surface. In addition, for very tiny metal nanoparticles, optical gradient force is a main part compared with scattering and absorption force.^{55,56} Under incident polarized light, the local electric field of silver nanoparticles was enhanced, under which some other silver atoms or particles were attracted due to optical gradient force along the dipole direction to form longer and bigger nanostructures. They are developed from nanoparticles to ripples and from ripples to nanoplates. This essentially coincides with what was reported by Tsuma that plasmon-induced charge separation at the interface between Ag

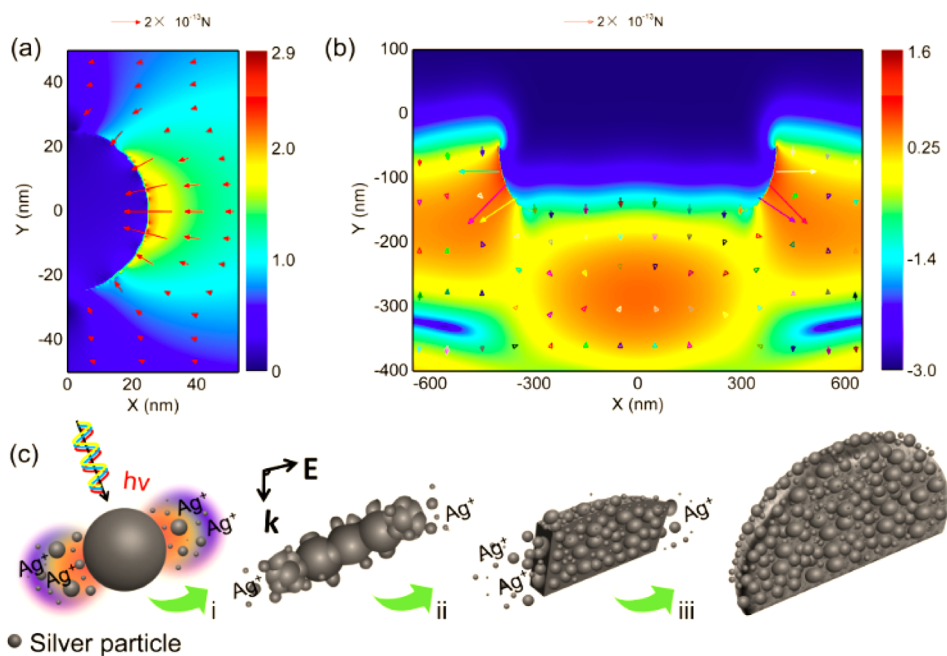


Figure 2. (a) E-field distribution of a 50 nm silver seed and gradient force for attracting silver atoms in the dipole of the silver seed. (b) E-field distribution of 300 nm ripples and gradient force for attracting silver atoms in the dipole of the silver ripple. (c) Proposed mechanism for the formation of silver nanoplates.

nanorods and TiO₂ was visualized by nanoscopic imaging of small satellite Ag nanoparticles deposited as a result of the charge separation. The charge separation sites as well as localized electric fields around the nanorods are distributed anisotropically depending on the excited plasmon modes, indicating that the charge separation is localized and is induced or promoted by the localized electric fields.^{48,49}

Figure 2 shows a simple estimation of the local electric field distribution around a 50 nm silver nanoparticle and a 300 nm silver ripple under excitation of an 800 nm laser. The electric field intensity increases when close to the surface of a silver nanoparticle/ripple which was demonstrated by the different colors in the near region (Figure 2a,b). The optical gradient force simulation is conducted to explain the process of the assembly of tiny clusters to form structures under the focused laser field. During the first-layer scanning process, a continuous nanoparticle film was formed and the size of the nanoparticles distributed around 50 nm, so we just chose a single 50 nm nanosphere as a simulated sample to explain the ripple formation based on nanoparticles in the second-layer scanning process in the next step. We suppose the simulated nanoparticle is relatively motionless and gave an enhancement of local electric field, under which the smaller clusters or ions were attracted to assemble in the end. Similarly, we simulated that a ripple grew longer to even form a nanoplate. We also attribute this attraction force to optical gradient force and use this simple model to show the assembly process directly during the formation of a single nanoplate. The optical gradient force of attraction exerted by a 1 nm silver

nanoparticle by electric field near a pole of the dipole may be as large as \sim pN, which is similar to a trapping force of 2 pN/W/ μm^2 (numerical result) exerted on a 50 nm diameter polystyrene bead in water that was reported through an analytical Lorentz force model.⁵⁷ The optical gradient force was shown as follows: $F = 1/2\alpha\nabla E^2$, where E is the intensity of the electric field and E^2 the laser intensity, α is the polarizability of a nanoparticle; the detailed optical attracting force model and calculation are given in the Supporting Information. Obviously, the gradient force increases with the distance between the atoms with the surface of the dipoles along the fixed axis, as demonstrated by the length of the red force arrows (Figure 2a,b). Although the single pulse duration is as short as 100 fs, the relatively low scanning speed, around 50 $\mu\text{m/s}$, and the finite focal spot size, \sim 500 nm in diameter, estimated from the Airy spot size, leads to a continuous crystal growth under irradiation for 1 ms, sufficient for diffusion of the surrounding ions and atoms (Figure 2c). Here, the incident ultrafast laser plays the roles of both photoreducing silver ions by multiphoton absorption and, in the meantime, exciting SPs to direct the construction of nanostructures. The initial silver seed layer formation by laser scanning is critical, which guarantees appropriate surface roughness to ensure efficient coupling of light to SP modes. Also, use of an oil-immersion high numerical aperture (NA, 1.40) objective lens is found to be indispensable for efficient SP coupling from the evanescent field built on a metal–solution interface, which constructs an Otto configuration prism coupling system (Figure S2).

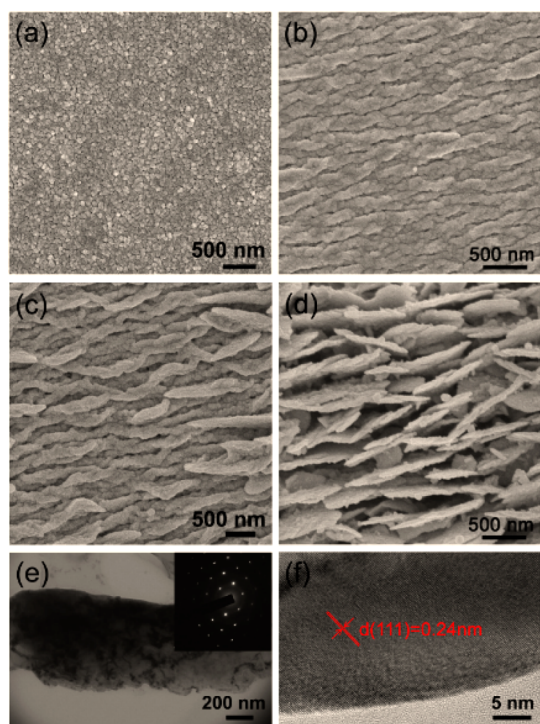


Figure 3. SEM of different outcomes during the process of formation of nanoplates through tightly focused femtosecond laser multilayer scanning process including different silver structures fabricated through tightly focused femtosecond laser multilayer scanning process. (a) Silver film composed of directed nanoseeds between 20 and 80 nm through single-layer scanning process. (b) Directed silver ripples through bilayer scanning process. (c) Ripples transformed to nanoplates through triple-layer scanning process. (d) Upright nanoplates fabricated through four or more than four-layer scanning process. (e) TEM image of a silver nanoplate; inset is the diffraction pattern. (f) HR-TEM image of the edge of the nanoplate.

The above scenario was proved by the surface feature evolution in different stages of nanoplate formation in our experiments. The detailed multilayer scanning process is shown as Figure S3. During the first-layer scanning process, the silver nanoparticles were photoreduced, where some with sizes of 20–80 nm were directly deposited on the surface of substrate (glass) to form a film (Figure 3a) and others suspended in the vicinity. SPs could be excited in the silver film that was sandwiched between a glass chip and precursor solution (insulator–metal–insulator, IMI). In the classical prism coupling scheme, SPs are confined to the proximity of the metal–dielectric interface and decay exponentially in both media. The fabricating system functions as an Otto configuration prism coupling system, sufficient to excite SPs at the interface between the metal and the lower-index precursory solution. SPs can be excited, for example, by a polarized light incident on metallic film from the side of a glass prism at the critical angle θ_{sp} at which the projection of the wave vector of the photon to the x axis, $k_x = k\sqrt{\epsilon} \sin \theta_{sp}$, is equal to k_{sp} , is inherently leaky waves which lose energy *via* absorption of the metal

and radiation into the lens (ϵ is the dielectric constant).⁵⁸ In this case, the laser focused by an oil-immersion objective lens propagates from optically dense medium (oil) to thinner medium (precursor solution–metal film interface) which could achieve prism coupling of SPs using attenuated total internal reflection.

In the subsequent second-layer scanning process, the ripples (Figure 3) were generated with subwavelength intervals of ~ 200 nm, which is much smaller, considering that the wavelength of the femtosecond laser is about 800 nm. To the best of our knowledge, the deep-subwavelength metal nanostructures produced by photoreduction growth of metal ions have not been reported. Resolution of 20 nm Pt patterns was achieved through photodeposition combined with mask assisting electron beam lithography.³⁰ We deem that these deep-subwavelength ripples were a synergistic effect by incident laser and excited SPs, which is similar to some periodic subwavelength structures made by laser ablation on the solid substrate of an insulator,⁵⁹ semiconductor,⁶⁰ or metals.⁶¹ The difference is that the ripples they observed has a perpendicular relationship with the polarization of lasers.⁶² The transition/appearance (Figure 3c) and formation (Figure 3d) of plates were also shown as different stage outcomes. According to the series of SEM images, the lengths of most of the nanoplates have values between 1 and 2 μm . A scraped-off silver nanoplate is shown in Figure 3e, which is about 800 nm high and 2 μm long. In order to investigate the crystalline structure of these silver nanoplates, the sample was also characterized by X-ray diffraction and high-resolution transmission electron microscopy (HR-TEM). The XRD spectra showed the classic diffraction peak related to the lattice of the (111), (200), and (220) planes (Figure S4). These three peaks were in accordance with the ones of Ag powder (Figure S5). The diffraction pattern of transmission electron microscopy (TEM) of the smooth border shows that the nanoplate is a cubic-phase single crystal (Figure 3e). In the HR-TEM image (Figure 3e,f), the lattices of the [111] plane of cubic-phase silver could be easily identified, and the interplanar spacing is measured to be 0.24 nm, in agreement with the theoretical value of 0.239 nm. Theoretical studies suggest that citrate binds more strongly to Ag(111) than to Ag(100) surfaces at room temperature, which fits well with these experimental results.⁶³ Because of the stronger binding of citrate, the [111] facets are expected to grow more slowly than the [100] facets when citrate ions are present. As a result, the [111] facets will become increasingly dominant on the surface.⁴³ In addition, some silver nanoparticles adhered to the surface of the nanoplate, and parts of the detection area showed the polycrystalline structures of the silver nanoparticles. As shown in Figure S6, the lattice of the (111) and (200) planes could be clearly identified from the image, confirming their polycrystalline

properties. The interplanar spacings of these two planes are 0.24 and 0.20 nm, respectively, which are very close to the theoretical values (0.236 and 0.201 nm). The inset of Figure 2d is the electron diffraction pattern of the rough area of this silver nanoplate, and the bright rings correspond to the (111), (200), (220), and (311) silver planes, confirming its polycrystalline structure.

During the first-layer scanning process, photochemical growth takes a leading role in controlling the shape and size of nanoparticle films that served as dipoles in the subsequent step; in the second, third, and more layer scanning steps, SPs begin to serve as a mediator to induce the ripple and plate patterns. This model is further evidenced by the polarization dependence experiment. The orientation of the plates was not found to be related to the scanning route in either the mansard route or the involute coil route but was determined by the polarization of the laser light. As shown by SEM images of a series of $8\ \mu\text{m} \times 15\ \mu\text{m}$ rectangles in Figure 4, nanoplates are always arrayed parallel to the laser polarization, as well as the electric field direction of light and silver dipoles, which are indicated by inset arrows in Figure 4. Rotation of the polarization of linear laser light causes sensitive corresponding change of the orientation of the upright

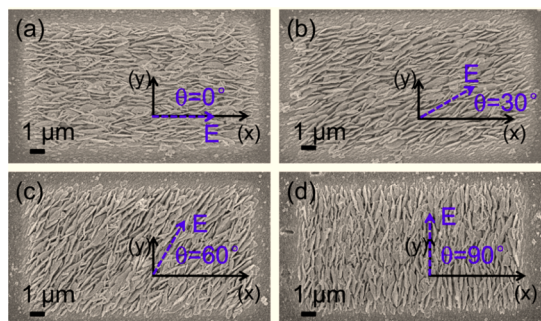


Figure 4. Effect of laser beam polarization on the orientation of silver nanoplates. (a–d) SEM images of silver hierarchical nanoplate array with different orientations by adjusting the laser polarization directions; the angles between the polarization direction and horizontal direction were 0, 30, 60, and 90°.

silver nanoplates. Figure 4a–d shows four different directions of nanoplate arrays, and the angle between nanoplate orientation and horizontal direction changed from 0° to 30, 60, and 90° when changing the direction of laser polarization. It is consistent with the axis characteristics of SPs induced by the enhanced local electric field. These results show the clear role of SPs excitation in the nanoplates' growth.

The concentration of silver precursor is also a vital issue for processing. The UV–visible absorption spectra of different concentrations of silver precursor are shown in Figure 5. Obviously, the absorption peaks were all at 302 nm, and the intensity increases with the concentration value accordingly. When the concentration value was too low, for example, the absorption peak nearly disappeared at 0.00166 M. The different concentrations of silver precursor have different laser threshold power to induce photoreaction. The silver ion concentration we applied in this article is 0.083 M, which we adopted as 0.02-, 0.1-, 0.5-, 5-, 10-, and 50-fold concentrations to study the threshold and mechanism. The threshold power and concentration dependence is shown in Figure 5a. The lower concentrations have higher threshold power. The threshold value corresponding to 0.083 M we used in the paper is 0.8 mW, and the threshold nearly does not change when the concentration is greater than 0.083 M. The silver structures were different under different concentrations. It is found that the nanoplates were difficult to produce, and the structures were even discontinuous or some ripples appeared with lower concentrations, which was influenced by the poor ion supply and delivery. When the concentration value is higher, the thickness of silver nanoplates increases, however, not so obviously compared with the change of the concentration of silver ions and the nanoplates that seem to adhere to small particles more easily (Figure S7). At the same time, the silver precursor at high concentration is easier to form a triangular nanoprism and truncated triangular nanoprism in solution. The deposited nanoparticles even go against the fabrication when the concentration value attains 0.45 mol/L

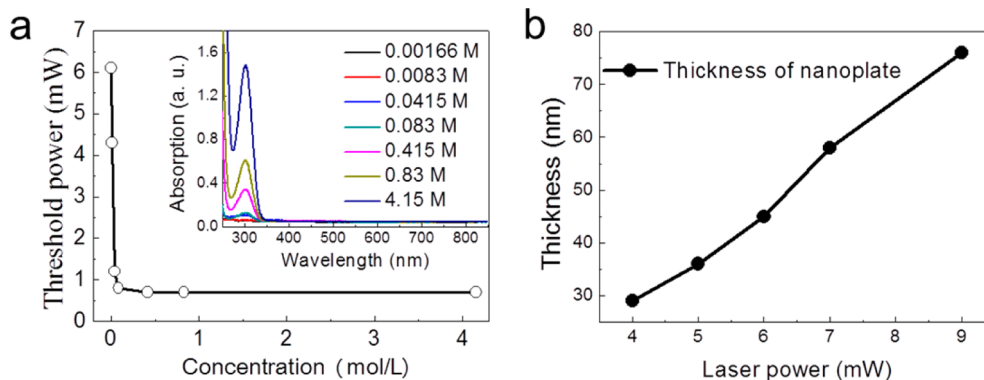


Figure 5. (a) Change of threshold power of photoreaction under different concentrations from 0.00166 to 4.15 M. (b) Nanoplates' thickness increasing with the laser power under a concentration of 0.083 M.

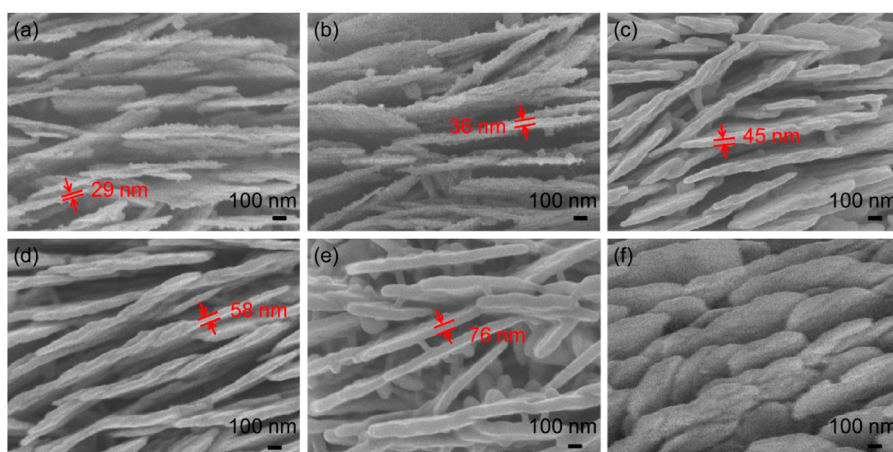


Figure 6. (a–e) SEM images of the nanoplates with different thicknesses under different laser power. (f) Lateral view of nanoplates in panel c.

(shown in Figure S8). This phenomenon coincides with the series of work on the silver prisms reported by Mirkin. The concentration of silver ions will influence the material delivery and the photoreduction process directly. The order of magnitude analysis of heat and mass transport induced by Marangoni convection was given. The analysis suggests that the laser-induced temperature distribution develops within 1 ms and Marangoni convection flow commences within 0.01–1 s, which increases by 1–2 orders of magnitude the mass transfer of dissolved molecules into the laser focus where they are trapped.⁶⁴ The diffusion coefficient of silver ions in water is $1.64 \times 10^{-9} \text{ m}^2/\text{s}$, and the delay for stabilization time for diffusion is $\sim 0.73\text{--}73 \text{ s}$. This suggests that the induced convection developed within $\sim 1.2 \times 10^{-3}$ to 0.12 s can play a very significant role. The extrapolated estimate shows that even in the case of $M_{\text{am}} = 4.18 \times 10^3$ ($D = 1.64 \times 10^{-9} \text{ m}^2/\text{s}$) this factor reaches $D_{\text{eff}}/D \approx 7$; that is, a very strong enhancement of mass transfer into the irradiated spot takes place. This means that during laser trapping the induced Marangoni convection significantly increases mass transfer within the area over which significant surface tension gradients exist.

With the SPs-mediated nanoplate directional growth model confirmed, more phenomena could be interpreted further. The larger laser intensity will provide more energy for forming larger nanoparticles as units which will construct thicker nanoplates. We fabricated a silver hemisphere, and a 3D structure is shown in Figure S9 by a 50-layer scanning process under different laser power. The thickness of the nanoplate increased with the applied laser power (Figure 5b). The values of the nanoplates' thicknesses are 29, 36, 45, 58, and 76 nm when applying a laser power of 4, 5, 6, 7, and 9 mW, and the SEM images of some different thickness values of silver nanoplates are shown in Figure 6a–e. The attractive force generated in the pole of the nanostructure is a mainly optical gradient force in the enhanced optical field. The optical

gradient force will accelerate with the laser power, and the assembly process of silver nanoparticles will also be enhanced. In addition, more photons will be provided under higher laser power, which will accelerate the photoreduction process of silver ions. Both of these two impacts of enhanced assembly and photoreduction process will increase the thickness of silver nanoplates. The thinnest line width achieved by laser direct writing through the TPA process was about 100 nm as previously reported. In contrast, the thickness of the nanoplate here was as small as $\lambda/27$ (λ , the writing laser wavelength) level, far beyond the optical diffraction limit, and it is obvious that SPs-mediated construction of metal structures could benefit from a lower limit line width and enhance the fabrication accuracy in optical nanofabrication. Through the lateral view of nanoplates (Figure 6f), we found that the surface of the nanoplates could still show a multiple state, which confirms that the nanoplates were formed due to the SPs-induced assembly of nanoparticles. So far, polarized femtosecond laser-induced photoreduction, growth, and programmable assembly of silver nanoparticles into nanoplates and micropatterns, during which the laser provides energy, excites SPs to assemble directly and achieve high space resolution, so we call it an optical dynamic assembly process.

It was also found that the nanoplates could be adhered with a series of nanoparticles, as shown in Figure 7. Statistical results show that the thickness of the upright nanoplates in Figure 7a is in the range of 30–70 nm with an average value of ~ 55 nm (Figure 7b). The diameter of the nanoparticles on the nanoplates is between 25 and 80 nm with a central value of ~ 50 nm (Figure 7c). These triply hierarchical nanoplates adhered with nanoparticles were provided as “hot spots” with an ultrahigh enhancement factor of 10^{11} with *p*-aminothiophenol (*p*-ATP) as the target molecule, with 514 nm laser as the excitation source (Figure 7d). The laser power of 10 mW combined with an elliptical spot size produced a power density of $0.1 \text{ kW}/\text{cm}^{-2}$. The typical accumulation time for each

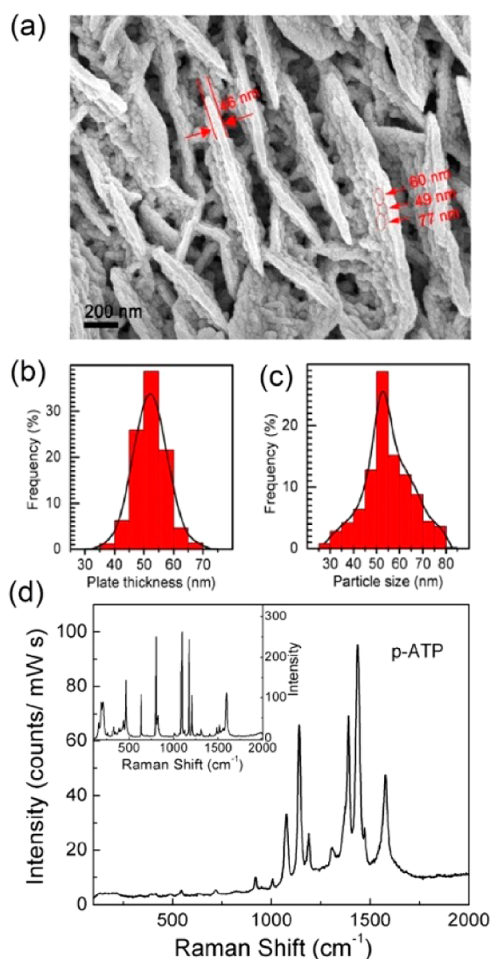


Figure 7. Structural characterization of the hierarchical silver substrate. (a) SEM image of the hierarchical silver substrate. (b) Thickness distribution of the nanoplates. (c) Size distribution of the nanoparticles. (d) SERS spectra of p-ATP molecules; the normalized intensity was gained by dividing the initial value by 10 mW and 10 s.

SERS measurement in this study was 10 s. By simulating an electric field of such adhered neighboring silver nanoparticles with the same diameter of 50 nm and with a gap of 1 nm, the enhanced electromagnetic field E can reach a value of 800 (Figure S10). The reproducible high enhancement factor should be associated with the fact that the SERS intensity is in direct proportion to the fourth power of the field strength, $|E|^4$. The 3D upright silver nanoplates will enhance the actual active surface, which is larger than the flat surface under the same size of the laser spot. The enhanced actual surface will benefit by absorbing more molecules, so the collected signals were enhanced relatively, which is also another advantage for SERS detection. So the enhancement factor of 10^{11} is based on both the enhanced actual absorbed surface and the rough silver nanostructures just as the silver island film. The rough surface of the nanoplate should result from the fact that photogenerated atoms or small nanoparticles were attracted to the dipoles along the dipole tips by optical gradient force in SP-enhanced electric field and also small particles adhered in the nanoplates through electrostatic force in the vertical direction of the dipole ends; in other words, the thickness and smoothness of the nanoplates were also influenced by electrostatic effect. The surfaces of silver nanoparticles were negatively charged because they were formed from silver ion solution with trisodium citrate acting as the capping agent. Citrate has three carboxylic groups, and it has been shown by Munro *et al.*⁶⁵ that mainly two of them would bind to the silver surface, leaving the third one normal to the surface and responsible for the colloid stabilization by electrostatic repulsion.⁴⁴ So the SPs-induced directional assembly of nanoparticles is a process of optical attraction force that vanquishes electrostatic repulsion. In addition, the silver

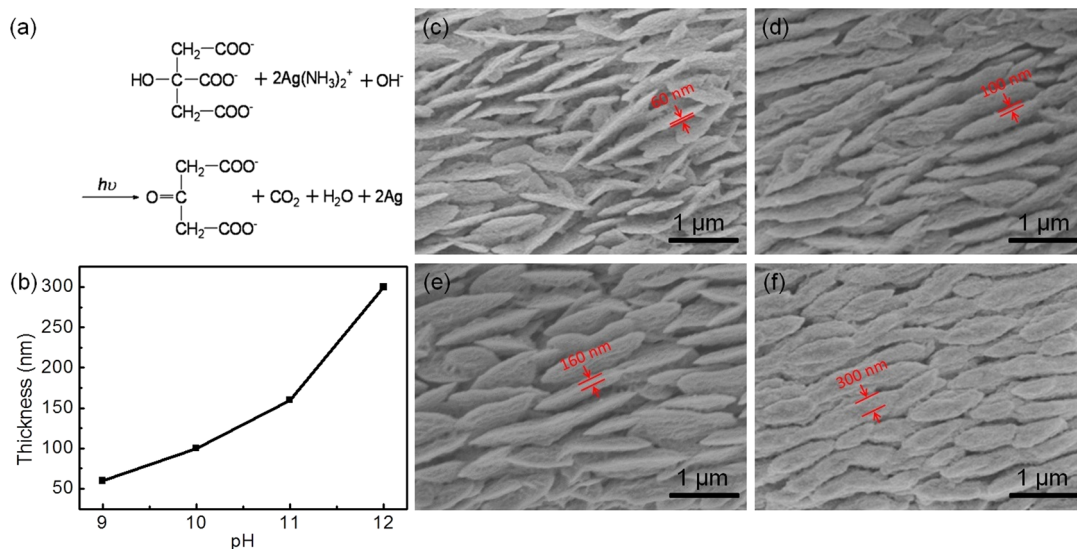


Figure 8. Thickness of silver nanoplates increases with the pH value of the precursor. (a) Photoreaction equation. (b) Nanoplate thickness increasing with the pH values. (c–f) SEM of different thickness of nanoplates with pH values of 10.8, 11, 11.5, and 12.

nanoparticle fusion is not efficient due to electrostatic repulsion, which gives rise to the rough surface.

The electrostatic force between nanoparticles depends on the charge number that was affected by the ionizing degree of capping agents when capped with a certain number of molecules. To clarify the electrostatic force effect, we adjust the pH value of the silver precursor with NaOH to study the changes of the nanoplates. We found that the thickness of nanoplates increased with the pH value from 10.8 to 12 (Figure 8b). However, the negative charges of the citrate anion increase with the pH of the solution. The increase of the negative charges will increase the electrostatic force and decrease the chance of nanoparticles adhering to the side surface of the nanoplate freely, which will influence the roughness of the nanoplate. On the other hand, the OH^- is necessary in the photoreduction of silver ions,^{22,66} and the related reaction equation is shown in Figure 8a. The main OH^- source comes from the ionization of ammonia, and the photoreduction process will be promoted when the pH value increases and the thickness of the nanoplates will increase, too. With pH 10 as an example, the concentration of $[\text{OH}^-]$ is about 10^{-4} M, and the precursor solution we used here is 6.3×10^{-2} M; according to the reaction equation, the $[\text{OH}^-]$ is relatively insufficient. When the pH value is near 12, the nanoplate is not only thicker but longer. The optical attracting mechanism will compete with the static repulsion force under high pH value. However, the silver ion precursor became muddy even with sediment, and the high concentration of OH^- resulted in the removal of silver ions from the precursor when the pH value exceeded 12, which blocks the photoreaction.

CONCLUSION

In summary, a surface-plasmon-mediated programmable optical nanofabrication method was demonstrated

on silver. Three critical steps, namely, (i) seed production; (ii) excitation and coupling of light to localized SPs modes and their mediation to the directional growth of nanoplates; and (iii) attraction of silver ions photoreduced on the surface of nanoparticles and attraction of early produced nanoparticle assembly in the dipole ends. During these steps, the polarized laser pulses provide energy, excite SPs to assemble directly, and achieve high space resolution. The silver nanoplate growth mechanism was clarified, and the SPs act as a direction guide for nanoplates growth, attract the silver ions, and provide the driving force to overcome the electrostatic repulsive force for nanoparticle assembly.

The micropattern shape and location, the nanoplate orientation, and the thickness are all attained in controlled fashion. The triply hierarchical nanoplate (adhered with nanoparticles) micropatterns were gained due to the inefficient fusion process between repulsive nanoparticles under high pH value. The laser power threshold decreases with the increase of the concentration of silver precursor, and the Marangoni convection significantly increases mass transfer within the area of laser focus. The probability of free combination between nanoparticles improved, and the thickness of the nanoplates increased from 60 to 300 nm when the pH value was changed from 10.8 to 12, during which the amount of OH^- source is an important issue for photoreduction of silver ions. The thickness of the nanoplate was as small as $\lambda/27$ (λ , the writing laser wavelength) level, far beyond the optical diffraction limit, and it is obvious that SPs-mediated construction of metal structures could benefit from lower limit line width and enhance the fabricating accuracy in optical nanofabrication. In the future, SPs-assisted metal optical nanofabrication technology with true 3D and high precision structure fabrication on nanoelectronic devices and optical metamaterials may find broad application.

METHODS AND MATERIALS

Materials. Silver nitrate (AgNO_3) and *p*-aminothiophenol (p-ATP) were purchased from Sigma-Aldrich Co., Ltd. Trisodium citrate ($\text{C}_6\text{H}_5\text{O}_6\text{Na}_3$), sodium hydroxide, and ammonia were purchased from Beijing Chemicals Co., Ltd. The silver precursor was prepared by dripping a suitable amount of aqueous ammonia onto a mixture of silver nitrate aqueous solution (0.083 mol^{-1}) and trisodium citrate (0.062 mol L^{-1}) under stirring until a clear solution was formed. The pH value of the precursor was adjusted by adding NaOH solution. The microchannel was fabricated on a normal glass substrate by using photolithography and wet etching techniques.

Femtosecond Laser Direct Writing Process. For each fabrication, the 800 nm femtosecond laser pulse, with a width of 120 fs and mode locked at 82 MHz (from Tsunami, Spectra Physics), was tightly focused by a high numerical aperture ($\text{NA} = 1.4$) oil-immersion objective lens ($100\times$). The laser power was controlled by a gradual neutral density filter. The focal spot was scanned laterally by steering a two galvano-mirror set and kept along the optical axis by a piezo stage, both with high motion accuracy. The silver nanoplates were fabricated with $1000 \mu\text{s}$

exposure duration at each dot. All of the processes of fabrication were controlled by a computer. The linear laser polarization direction was adjusted based on Glan prism and a half-wave plate.

Simulation. The optical electric field distribution of the nanoparticle and nanoripple excited by an 800 nm wavelength light was simulated by the finite difference time domain method; the optical gradient force distribution was gained through MATLAB (Matrix Laboratory), and the gradient force was calculated according to this formula:⁵⁵

$$F_{\text{grad}} = \frac{|\alpha|}{2} \nabla \langle E^2 \rangle \quad (1)$$

Characterization. The absorption spectra were measured on a Shimadzu UV-3600 spectrometer. The surface morphologies of the samples were measured on a JEOL JSM-6700F field emission scanning electron microscope operating at 3.0 keV. The crystalline structure of the samples was characterized by a JEOL-2100F HR-TEM functioning at 200 kV. Surface-enhanced Raman spectra were measured on JOBIN YVON T64000 equipped with a liquid-nitrogen-cooled argon ion laser at 514.5 nm (Spectra-Physics

Stabilite 2017) as excitation source (the laser power used was about 40 μ W at the samples with an average spot size of 1 μ m in diameter). The spectral resolution was 4 cm^{-1} at the excitation wavelength.

Conflict of Interest: The authors declare no competing financial interest.

Acknowledgment. The authors gratefully acknowledge support from 973 project (Grant Nos. 2011CB013003 and 2013CBA01700), and National Science Foundation of China (NSFC) (Grant Nos. 51335008, 61378053, and 61377048). This work is also supported by 2010 Ph.D. interdisciplinary project No. 450091102507, Jilin University.

Supporting Information Available: Absorption of silver precursor, the highly focused laser beam exciting SPs, the layer-by-layer scanning process, the hierarchical silver nanoplate, the estimation of enhancement factor, and the enhanced electromagnetic field E of the adhered nanoparticles. This material is available free of charge via the Internet at <http://pubs.acs.org>.

REFERENCES AND NOTES

1. Cho, W. J.; Kim, Y.; Kim, J. K. Ultrahigh-Density Array of Silver Nanoclusters for SERS Substrate with High Sensitivity and Excellent Reproducibility. *ACS Nano* **2011**, *6*, 249–255.
2. Zhu, Z.; Meng, H.; Liu, W.; Liu, X.; Gong, J.; Qiu, X.; Jiang, L.; Wang, D.; Tang, Z. Superstructures and SERS Properties of Gold Nanocrystals with Different Shapes. *Angew. Chem., Int. Ed.* **2011**, *50*, 1593–1596.
3. Sun, M.; Zhang, Z.; Wang, P.; Li, Q.; Ma, F.; Xu, H. Remotely Excited Raman Optical Activity Using Chiral Plasmon Propagation in Ag Nanowires. *Light: Sci. Appl.* **2013**, *2*, e112.
4. Gervinskis, G.; Seniutinas, G.; Hartley, J. S.; Kandasamy, S.; Stoddart, P. R.; Fahim, N. F.; Juodkazis, S. Surface-Enhanced Raman Scattering Sensing on Black Silicon. *Ann. Phys.* **2013**, *525*, 907–914.
5. Yokota, Y.; Ueno, K.; Juodkazis, S.; Mizeikis, V.; Murazawa, N.; Misawa, H.; Kasa, H.; Kintaka, K.; Nishii, J. Nano-textured Metallic Surfaces for Optical Sensing and Detection Applications. *J. Photochem. Photobiol. A* **2009**, *207*, 126–134.
6. Fleischer, M.; Weber-Bargioni, A.; Altoe, M. V. P.; Schwartzberg, A. M.; Schuck, P. J.; Cabrini, S.; Kern, D. P. Gold Nanocone Near-Field Scanning Optical Microscopy Probes. *ACS Nano* **2011**, *5*, 2570–2579.
7. Kawata, S.; Inouye, Y.; Verma, P. Plasmonics for Near-Field Nano-imaging and Superlensing. *Nat. Photonics* **2009**, *3*, 388–394.
8. Torimoto, T.; Horibe, H.; Kameyama, T.; Okazaki, K.-i.; Ikeda, S.; Matsumura, M.; Ishikawa, A.; Ishihara, H. Plasmon-Enhanced Photocatalytic Activity of Cadmium Sulfide Nanoparticle Immobilized on Silica-Coated Gold Particles. *J. Phys. Chem. Lett.* **2011**, *2*, 2057–2062.
9. Odom, T. W.; Schatz, G. C. Introduction to Plasmonics. *Chem. Rev.* **2011**, *111*, 3667–3668.
10. Stewart, M. E.; Anderton, C. R.; Thompson, L. B.; Maria, J.; Gray, S. K.; Rogers, J. A.; Nuzzo, R. G. Nanostructured Plasmonic Sensors. *Chem. Rev.* **2008**, *108*, 494–521.
11. De Angelis, F.; Gentile, F.; Mecarini, F.; Das, G.; Moretti, M.; Candeloro, P.; Coluccio, M. L.; Cojoc, G.; Accardo, A.; Liberale, C.; et al. Breaking the Diffusion Limit with Super-hydrophobic Delivery of Molecules to Plasmonic Nanofocusing SERS Structures. *Nat. Photonics* **2011**, *5*, 682–687.
12. Ebbesen, T. W.; Lezec, H. J.; Ghaemi, H. F.; Thio, T.; Wolff, P. A. Extraordinary Optical Transmission through Sub-wavelength Hole Arrays. *Nature* **1998**, *391*, 667–669.
13. Masuda, H.; Fukuda, K. Ordered Metal Nanohole Arrays Made by a Two-Step Replication of Honeycomb Structures of Anodic Alumina. *Science* **1995**, *268*, 1466–1468.
14. Grier, D. G. A Revolution in Optical Manipulation. *Nature* **2003**, *424*, 810–816.
15. Fedoruk, M.; Lutich, A. A.; Feldmann, J. Subdiffraction-Limited Milling by an Optically Driven Single Gold Nanoparticle. *ACS Nano* **2011**, *5*, 7377–7382.
16. Kumar, K.; Lee, K. K. C.; Li, J.; Nogami, J.; Kherani, N. P.; Herman, P. R. Quantized Structuring of Transparent Films with Femtosecond Laser Interference. *Light: Sci. Appl.* **2014**, *3*, e157.
17. Shukla, S.; Vidal, X.; Furlani, E. P.; Swihart, M. T.; Kim, K.-T.; Yoon, Y.-K.; Urbas, A.; Prasad, P. N. Subwavelength Direct Laser Patterning of Conductive Gold Nanostructures by Simultaneous Photopolymerization and Photoreduction. *ACS Nano* **2011**, *5*, 1947–1957.
18. Zhang, Y.-L.; Chen, Q.-D.; Xia, H.; Sun, H.-B. Designable 3D Nanofabrication by Femtosecond Laser Direct Writing. *Nano Today* **2010**, *5*, 435–448.
19. Kawata, S.; Sun, H.-B.; Tanaka, T.; Takada, K. Finer Features for Functional Microdevices. *Nature* **2001**, *412*, 697–698.
20. Obata, K.; El-Tamer, A.; Koch, L.; Hinze, U.; Chichkov, B. N. High-Aspect 3D Two-Photon Polymerization Structuring with Widened Objective Working Range (Wow-2pp). *Light: Sci. Appl.* **2013**, *2*, e116.
21. Sun, Y.-L.; Dong, W.-F.; Niu, L.-G.; Jiang, T.; Liu, D.-X.; Zhang, L.; Wang, Y.-S.; Chen, Q.-D.; Kim, D.-P.; Sun, H.-B. Protein-Based Soft Micro-optics Fabricated by Femtosecond Laser Direct Writing. *Light: Sci. Appl.* **2014**, *3*, e129.
22. Xu, B.-B.; Xia, H.; Niu, L.-G.; Zhang, Y.-L.; Sun, K.; Chen, Q.-D.; Xu, Y.; Lv, Z.-Q.; Li, Z.-H.; Misawa, H.; et al. Flexible Nanowiring of Metal on Nonplanar Substrates by Femtosecond-Laser-Induced Electroless Plating. *Small* **2010**, *6*, 1762–1766.
23. Wu, D.; Niu, L.-G.; Chen, Q.-D.; Wang, R.; Sun, H.-B. High Efficiency Multilevel Phase-Type Fractal Zone Plates. *Opt. Lett.* **2008**, *33*, 2913–2915.
24. Juodkazis, S.; Mizeikis, V.; Misawa, H. Three-Dimensional Microfabrication of Materials by Femtosecond Lasers for Photonics Applications. *J. Appl. Phys.* **2009**, *106*, 051101.
25. Xia, H.; Wang, J.; Tian, Y.; Chen, Q.-D.; Du, X.-B.; Zhang, Y.-L.; He, Y.; Sun, H.-B. Ferrofluids for Fabrication of Remotely Controllable Micro-nanomachines by Two-Photon Polymerization. *Adv. Mater.* **2010**, *22*, 3204–3207.
26. Wang, J.; He, Y.; Xia, H.; Niu, L.-G.; Zhang, R.; Chen, Q.-D.; Zhang, Y.-L.; Li, Y.-F.; Zeng, S.-J.; Qin, J.-H.; et al. Embellishment of Microfluidic Devices via Femtosecond Laser Micronanofabrication for Chip Functionalization. *Lab Chip* **2010**, *10*, 1993–1996.
27. Sugioka, K.; Cheng, Y. Ultrafast Lasers—Reliable Tools for Advanced Materials Processing. *Light: Sci. Appl.* **2014**, *3*, e149.
28. Malinauskas, M.; Farsari, M.; Piskarskas, A.; Juodkazis, S. Ultrafast Laser Nanostructuring of Photopolymers: A Decade of Advances. *Phys. Rep.* **2013**, *533*, 1–31.
29. Ishikawa, A.; Tanaka, T.; Kawata, S. Improvement in the Reduction of Silver Ions in Aqueous Solution Using Two-Photon Sensitive Dye. *Appl. Phys. Lett.* **2006**, *89*, 113102.
30. Juodkazis, S.; Yamaguchi, A.; Ishii, H.; Matsuo, S.; Takagi, H.; Misawa, H. Photo-electrochemical Deposition of Platinum on TiO₂ with Resolution of Twenty Nanometers Using a Mask Elaborated with Electron-Beam Lithography. *Jpn. J. Appl. Phys.* **2001**, *40*, 4246.
31. Barnes, W. L.; Dereux, A.; Ebbesen, T. W. Surface Plasmon Subwavelength Optics. *Nature* **2003**, *424*, 824–830.
32. Hao, X.; Kuang, C.; Gu, Z.; Wang, Y.; Li, S.; Ku, Y.; Li, Y.; Ge, J.; Liu, X. From Microscopy to Nanoscopy via Visible Light. *Light: Sci. Appl.* **2013**, *2*, e108.
33. Dondapati, S. K.; Sau, T. K.; Hrelescu, C.; Klar, T. A.; Stefani, F. D.; Feldmann, J. Label-Free Biosensing Based on Single Gold Nanostars as Plasmonic Transducers. *ACS Nano* **2010**, *4*, 6318–6322.
34. Ruach-Nir, I.; Bendikov, T. A.; Doron-Mor, I.; Barkay, Z.; Vaskevich, A.; Rubinstein, I. Silica-Stabilized Gold Island Films for Transmission Localized Surface Plasmon Sensing. *J. Am. Chem. Soc.* **2006**, *129*, 84–92.
35. Ahn, W.; Boriskina, S. V.; Hong, Y.; Reinhard, B. M. Photonic–Plasmonic Mode Coupling in On-Chip Integrated Optoplasmonic Molecules. *ACS Nano* **2011**, *6*, 951–960.
36. Merlein, J.; Kahl, M.; Zuschlag, A.; Sell, A.; Halm, A.; Boneberg, J.; Leiderer, P.; Leitenstorfer, A.; Bratschkitsch, R. Nanomechanical Control of an Optical Antenna. *Nat. Photonics* **2008**, *2*, 230–233.

37. Savasta, S.; Saija, R.; Ridolfo, A.; Di Stefano, O.; Denti, P.; Borghese, F. Nanopolaritons: Vacuum Rabi Splitting with a Single Quantum Dot in the Center of a Dimer Nanoantenna. *ACS Nano* **2010**, *4*, 6369–6376.
38. Wang, Y.; Chen, J.; Irudayaraj, J. Nuclear Targeting Dynamics of Gold Nanoclusters for Enhanced Therapy of HER2+ Breast Cancer. *ACS Nano* **2011**, *5*, 9718–9725.
39. Yang, J.; You, J.; Chen, C.-C.; Hsu, W.-C.; Tan, H.-R.; Zhang, X. W.; Hong, Z.; Yang, Y. Plasmonic Polymer Tandem Solar Cell. *ACS Nano* **2011**, *5*, 6210–6217.
40. Choi, H.; Chen, W. T.; Kamat, P. V. Know Thy Nano Neighbor. Plasmonic versus Electron Charging Effects of Metal Nanoparticles in Dye-Sensitized Solar Cells. *ACS Nano* **2012**, *6*, 4418–4427.
41. Lee, S. Y.; Hung, L.; Lang, G. S.; Cornett, J. E.; Mayergoyz, I. D.; Rabin, O. Dispersion in the SERS Enhancement with Silver Nanocube Dimers. *ACS Nano* **2010**, *4*, 5763–5772.
42. Schmucker, A. L.; Harris, N.; Banholzer, M. J.; Blaber, M. G.; Osberg, K. D.; Schatz, G. C.; Mirkin, C. A. Correlating Nanorod Structure with Experimentally Measured and Theoretically Predicted Surface Plasmon Resonance. *ACS Nano* **2010**, *4*, 5453–5463.
43. Rycenga, M.; Cogley, C. M.; Zeng, J.; Li, W.; Moran, C. H.; Zhang, Q.; Qin, D.; Xia, Y. Controlling the Synthesis and Assembly of Silver Nanostructures for Plasmonic Applications. *Chem. Rev.* **2011**, *111*, 3669–3712.
44. Zhang, J.; Li, S.; Wu, J.; Schatz, G. C.; Mirkin, C. A. Plasmon-Mediated Synthesis of Silver Triangular Bipyramids. *Angew. Chem., Int. Ed.* **2009**, *48*, 7787–7791.
45. Jin, R.; Charles Cao, Y.; Hao, E.; Métraux, G. S.; Schatz, G. C.; Mirkin, C. A. Controlling Anisotropic Nanoparticle Growth through Plasmon Excitation. *Nature* **2003**, *425*, 487–490.
46. Langille, M. R.; Zhang, J.; Mirkin, C. A. Plasmon-Mediated Synthesis of Heterometallic Nanorods and Icosahedra. *Angew. Chem., Int. Ed.* **2011**, *50*, 3543–3547.
47. Yoo, H.; Millstone, J. E.; Li, S.; Jang, J.-W.; Wei, W.; Wu, J.; Schatz, G. C.; Mirkin, C. A. Core–Shell Triangular Bifrustums. *Nano Lett.* **2009**, *9*, 3038–3041.
48. Kazuma, E.; Sakai, N.; Tatsuma, T. Nanoimaging of Localized Plasmon-Induced Charge Separation. *Chem. Commun.* **2011**, *47*, 5777–5779.
49. Kazuma, E.; Matsubara, K.; Kelly, K. L.; Sakai, N.; Tatsuma, T. Bi- and Uniaxially Oriented Growth and Plasmon Resonance Properties of Anisotropic Ag Nanoparticles on Single Crystalline TiO₂ Surfaces. *J. Phys. Chem. C* **2009**, *113*, 4758–4762.
50. Ueno, K.; Juodkakis, S.; Shibuya, T.; Yokota, Y.; Mizeikis, V.; Sasaki, K.; Misawa, H. Nanoparticle Plasmon-Assisted Two-Photon Polymerization Induced by Incoherent Excitation Source. *J. Am. Chem. Soc.* **2008**, *130*, 6928–6929.
51. Geldhauser, T.; Ikegaya, S.; Kolloch, A.; Murazawa, N.; Ueno, K.; Boneberg, J.; Leiderer, P.; Scheer, E.; Misawa, H. Visualization of Near-Field Enhancements of Gold Triangles by Nonlinear Photopolymerization. *Plasmonics* **2011**, *6*, 207–212.
52. Otto, A. Excitation of Nonradiative Surface Plasma Waves in Silver by the Method of Frustrated Total Reflection. *Z. Phys.* **1968**, *216*, 398–410.
53. Henglein, A. Colloidal Silver Nanoparticles: Photochemical Preparation and Interaction with O₂, CCl₄, and Some Metal Ions. *Chem. Mater.* **1998**, *10*, 444–450.
54. Maillard, M.; Huang, P.; Brus, L. Silver Nanodisk Growth by Surface Plasmon Enhanced Photoreduction of Adsorbed [Ag⁺]. *Nano Lett.* **2003**, *3*, 1611–1615.
55. Xu, B.-B.; Zhang, R.; Wang, H.; Liu, X.-Q.; Wang, L.; Ma, Z.-C.; Chen, Q.-D.; Xiao, X.-Z.; Han, B.; Sun, H.-B. Laser Patterning of Conductive Gold Micronanostructures from Nanodots. *Nanoscale* **2012**, *4*, 6955–6958.
56. Svoboda, K.; Block, S. M. Optical Trapping of Metallic Rayleigh Particles. *Opt. Lett.* **1994**, *19*, 930–932.
57. Seniutinas, G.; Rosa, L.; Gervinskas, G.; Brasselet, E.; Juodkakis, S. 3D Nano-structures for Laser Nano-manipulation. *Beilstein J. Nanotechnol.* **2013**, *4*, 534–541.
58. Maier, S. A. *Plasmonics: Fundamentals and Applications*; Springer: New York, 2007.
59. Shimotsuma, Y.; Kazansky, P. G.; Qiu, J.; Hirao, K. Self-Organized Nanogratings in Glass Irradiated by Ultrashort Light Pulses. *Phys. Rev. Lett.* **2003**, *91*, 247405.
60. Huang, M.; Zhao, F.; Cheng, Y.; Xu, N.; Xu, Z. Mechanisms of Ultrafast Laser-Induced Deep-Subwavelength Gratings on Graphite and Diamond. *Phys. Rev. B* **2009**, *79*, 125436.
61. Vorobyev, A. Y.; Makin, V. S.; Guo, C. Periodic Ordering of Random Surface Nanostructures Induced by Femtosecond Laser Pulses on Metals. *J. Appl. Phys.* **2007**, *101*, 034903.
62. Buividas, R.; Rosa, L.; Šliupas, R.; Kudrius, T.; Šlekys, G.; Datsyuk, V.; Juodkakis, S. Mechanism of Fine Ripple Formation on Surfaces of (Semi)Transparent Materials via a Half-Wavelength Cavity Feedback. *Nanotechnology* **2011**, *22*, 055304.
63. Kilin, D. S.; Prezhdo, O. V.; Xia, Y. Shape-Controlled Synthesis of Silver Nanoparticles: *Ab Initio* Study of Preferential Surface Coordination with Citric Acid. *Chem. Phys. Lett.* **2008**, *458*, 113–116.
64. Louchev, O. A.; Juodkakis, S.; Murazawa, N.; Wada, S.; Misawa, H. Coupled Laser Molecular Trapping, Cluster Assembly, and Deposition Fed by Laser-Induced Marangoni Convection. *Opt. Express* **2008**, *16*, 5673–5680.
65. Munro, C. H.; Smith, W. E.; Garner, M.; Clarkson, J.; White, P. C. Characterization of the Surface of a Citrate-Reduced Colloid Optimized for Use as a Substrate for Surface-Enhanced Resonance Raman Scattering. *Langmuir* **1995**, *11*, 3712–3720.
66. Xue, C.; Métraux, G. S.; Millstone, J. E.; Mirkin, C. A. Mechanistic Study of Photomediated Triangular Silver Nanoprism Growth. *J. Am. Chem. Soc.* **2008**, *130*, 8337–8344.